SAND2022-7366C

Development of Hierarchical Control for a Lunar Habitat DC Microgrid Model Using Power Hardware-in-the-Loop

Andrew R. R. Dow[1], Rachid Darbali-Zamora[1], Jack D. Flicker[1], Felipe Palacios II[1], and Jeffrey T. Csank[2]

[1]Sandia National Laboratories, Albuquerque, New Mexico, 87185, USA
[2]NASA Glenn Research Center, Cleveland, Ohio, 44135, USA

***Abstract* – As interest in space exploration grows, developing a lunar habitat has become a key component of extending missions into deep space. To guarantee reliable power management of a lunar habitat's DC microgrid, control schemes are needed that can manage the different assets (batteries, photovoltaics, loads) effectively. Proposed hierarchical control schemes are further developed into hardware solutions using Opal-RT's real-time simulation software and Power Hardware-in-the-Loop platform. Experimental results of a simulated DC microgrid and physical DC/DC components can allow better realization and performance of applications such as battery discharge control.**

Keywords* – *photovoltaics, DC microgrids, controls, power electronics, Opal-RT, lunar habitat, PHIL, DC/DC, energy storage

I. Introduction

NASA's Artemis Plan outlines the key objectives and elements of establishing a lunar base for short and long-term habitation on Earth's moon. Lunar habitation is a steppingstone towards deeper space exploration, with missions to Mars planned in the 2030s that will require a sustainable living environment on the planet's surface [3]. A major component of a lunar habitat will be its electrical power system. To sustain a permanent presence on Earth's moon, a highly reliable and ever-evolving power infrastructure will be needed that can withstand harsh environmental conditions, be extremely resilient, and easily expandable [2]. While some existing research does focus on power architectures for spacecrafts and satellites [5-8], power systems developed specifically for lunar habitation are less common and require further investigation. Typical power systems for space applications consider photovoltaic (PV) arrays as the primary power source, providing abundant renewable energy through solar irradiance exposure and maximum power point tracking (MPPT) conversion algorithms [9]. Battery Energy Storage Systems (BESS) can provide auxiliary power when PV is not adequately available [10]. This can occur during periods of eclipse, system failure, or heavy load demand. The BESS is crucial towards providing resiliency and stability in the lunar habitat power architecture.

Hierarchical control schemes for the BESS can be employed to achieve a more resilient power architecture than localized control alone. Due to varying line impedances across a power bus, differences in BESS performance, and environmental conditions, one can expect varying discharges rates between BESS units. Lack of uniformity in battery discharge can lead to power quality and reliability issues over time [1]. Hierarchical control can help achieve uniform discharge from all BESS modules by providing coordinated control on top of each module's local control strategy (droop control, voltage regulation, etc.) [11]. One proposed approach to hierarchical control defines three levels to optimize the distributed BESS power flow [1, 4]. While these studies highlight some key aspects at the simulation level, there is a need for implementing this control with hardware and testing under realistic conditions to further develop the solution.

Herein, a hierarchical control for a DC microgrid is implemented in a real-time simulation model using Opal-RT's RT-Labs. The hierarchical control for the BESS will ensure proper operations under varying PV and system conditions. The control scheme has been tested on a hardware DC/DC converter using a Power Hardware-in-the-Loop (PHIL) platform. Experimental results demonstrate the dynamic performance of the DC/DC converter operating under a hierarchical control scheme when the real-time simulation model is subjected to varying irradiance and load conditions.

II. DC Power Hardware-in-the-Loop Setup

To further investigate hierarchical control methods within the lunar habitat microgrid application, a PHIL platform consisting of a real-time simulation model and a hardware DC/DC converter are employed. The DC/DC converter functions as the battery charge-discharge unit (BCDU), regulating power between two DC source-load supplies. The current measurements of the BESS/BCDU are relayed to the real-time simulation through the Opal-RT's analog interface. Based on these values, the hierarchical control will determine how much power the DC/DC power converter should sink/source. Fig. 1 illustrates a block diagram of the experimental PHIL platform.

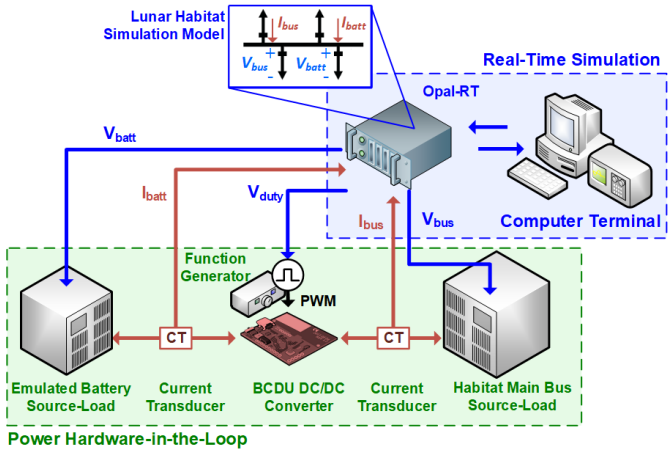

Fig. 1. Block Diagram for the Power Hardware-in-the-Loop Setup.

A. Opal-RT Real-Time Simulator

The Opal-RT OP5600 is a real-time simulation platform capable of integrating simulation models into PHIL testing. For this study, the lunar habitat model is developed in *MATLAB/Simulink* and integrated into RT-Labs for compiling and loading into the real-time processor. RT-Labs allows for control over the simulation during run-time as well as capturing and logging real-time data throughout the simulation. Furthermore, the Opal-RT provides an analog-to-digital interface for the various hardware signals. Current measurements, voltage setpoints, and control signaling can be interfaced between the real-time simulation model and hardware devices. The Opal-RT system relies on a discrete 40 µs timestep for input/output sampling time and real-time model operation.

B. BCDU Hardware Converter

The BCDU DC/DC converter consists of an evaluation module set designed and manufactured by Texas Instruments. The LMG34XX-BB-EVM and LMG3411EVM-018 operate as a synchronous half-bridge rectifier and gate driver/filter motherboard [17]. This evaluation module set is capable of bidirectional current flow (up to +/-8 A_{DC}) and step up/down voltage conversion (up to +480 V_{HI}). This DC/DC converter accepts a +5 V TTL square wave as its PWM switch waveform to control the half-bridge rectifier's gate drivers. The evaluation kit is assembled into a printed enclosure including fans for heat dissipation and insulated connectors for safety. Building the converter into an enclosure allows for a streamlined test setup and integration of this converter into a multitude of test environments.

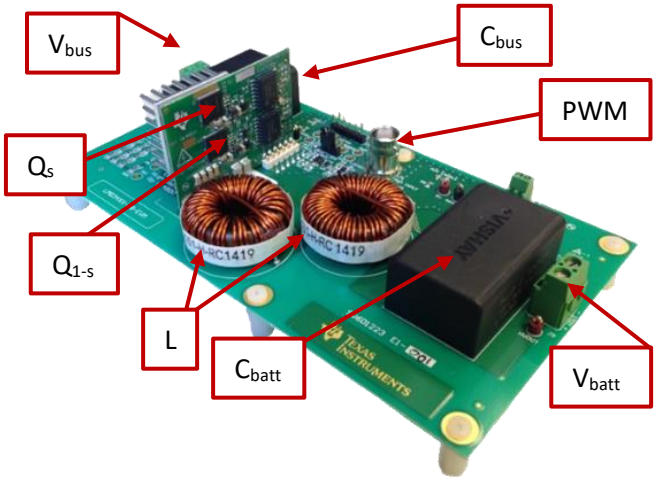

Fig. 2. TI LMG34XX Half-Bridge Bidirectional Converter [17].

C. PWM Generator

The PWM signal to the converter board is driven by a Teledyne LeCroy WaveStation 3162 function generator operating as a 100 kHz TTL square wave with a controlled, variable duty cycle. The function generator features an analog input capable of modulating the duty cycle of the PWM signal relative to the input signal's amplitude (+/-6 Vp = +/-5%). A nominal duty cycle for the BCDU is set with the real-time simulation either increasing or decreasing it based on the controller output.

D. Source-Load Power Supplies

The BCDU converter is connected to two Chroma 62180D source-load DC power supplies. These DC power supplies are capable of both sourcing and sinking current though the converter and can be voltage-controlled via analog set signals. The analog voltage set signals provided to each Chroma from the Opal-RT represent 1) an emulated battery voltage and 2) the main bus voltage for which the BCDU is connected to. Based on the control scheme of the converter and system voltages, power is transferred between the two supplies, through the BCDU, to support the main bus load and charge/discharge the battery.

E. Current Transducers

Finally, the current being fed from each source-load supply is measured using two AAC 929-50 bidirectional current transducers (CTs). The CTs provide a voltage output proportional to the current passing through the sensor. This voltage is fed into the Opal-RT's analog input and injected into the real-time simulation as a controlled current source. The hardware converter's behavior becomes integrated into the lunar habitat simulation model, contributing to the overall power source and consumption. To provide significant power from the hardware BCDU, the current signals measured in hardware are scaled up by a factor of 10x. This scaling allows the power levels from the BCDU hardware converter to be perceived as equivalent to the higher-power simulation models. To limit noise interference from the test environment and switching converter, low-pass filters are implemented in hardware and software on the current measurements.

III. Lunar Habitat Simulation Model

The lunar habitat simulation model consists of two subsystems: the solar array field (SAF) and the habitat. Power is sourced from the SAF's two PV arrays via solar array regulators (SAR) as well as two local BESS units (A, B). A BESS is comprised of a battery unit (BU) and BCDU capable of sourcing and sinking power based on load demand and solar array (SA) generation.

Power is sourced to the lunar habitat's DC-DC converter units (DDCU) and power distribution units (PDUs) for habitat load consumption. Two BESS units (C, D) are local to the lunar habitat alongside the power sourced from the SAF through the lunar habitat's local interconnect. A small impedance is introduced into the connection between the SAF and the lunar habitat to model the line losses present between the two subsystems. This line impedance is modeled as a lumped element, with a series resistor, inductor, and a shunt capacitor to ground.

The lunar habitat simulation model is implemented utilizing state-space average models that represent the dynamic behavior of the SAR, BCDU, and DDCU converters [9]. The simulation model is developed using *MATLAB/Simulink* with state-space average equations for each DC/DC converter model, alongside the *Simscape* Specialized Power Systems and standard library components. Fig. 3 illustrates a one-line diagram of the lunar habitat.

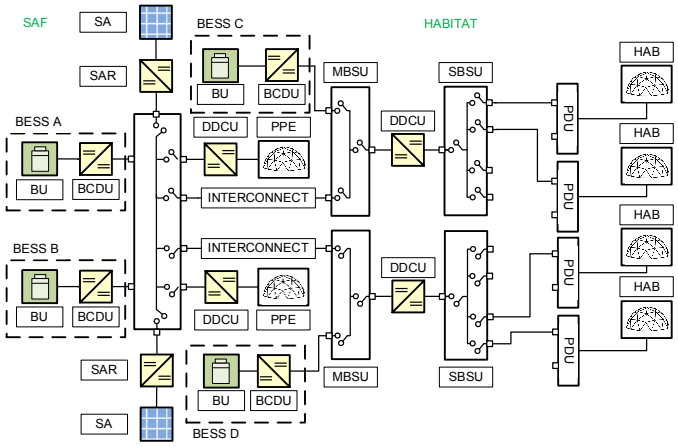

Fig. 3. One-line Diagram for the Lunar Habitat.

A. Solar Array (SA)

A dynamic mathematical PV model is used to represents the lunar habitat's SA [18]. This mathematical PV model allows varying irradiance and temperature conditions. Moreover, this model only requires the information provided from the PV manufacturer data sheet. The selected parameters provide adequate load and BESS charging power under full-irradiance conditions. Table I summarizes the parameters for the SA model used in the lunar habitat simulation model.

TABLE I:
SOLAR ARRAY SYSTEM PARAMETERS

Variable	*Description*	*Value*	*Unit*
N_{series}	*# of Panels in Series*	40	-
$N_{parallel}$	*# of Panels in Parallel*	230	-
V_{OC}	*Panel Open-Circuit Voltage*	5	*V*
I_{SC}	*Panel Short-Circuit Current*	0.35	*A*
$E_{e,nom}$	*Nominal Irradiance*	1000	Wm^{-2}
P_{NOM}	*Power at Nom. Irradiance*	18	*kW*
b	*Characteristic Constant*	0.0615	-

B. Solar Array Regulator (SAR)

A Single Ended Primary Inductor Converter (SEPIC) acts as the SAR for power conversion between the SA and the lunar habitat main bus voltage. The SEPIC is tasked with executing the optimal duty ratio MPPT algorithm to extract the utmost available power from the SA [16]. This algorithm provides the maximum power to the main bus from the SA by varying the output current for a given main bus voltage. The SEPIC topology is composed of two inductors, two capacitors, a diode, and a switching transistor. Fig. 4 illustrates the SEPIC topology circuit schematic.

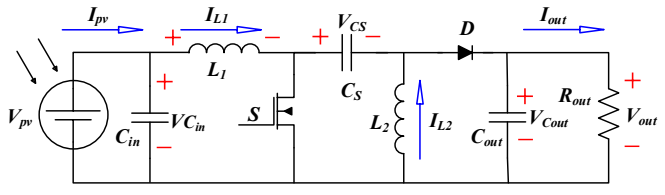

Fig. 4. The SEPIC circuit schematic. The SEPIC allows for lower, equal, or greater voltage levels at its output.

Performing an analysis on the ON and OFF switching states of the SEPIC, the dynamic equations can be obtained. The state equations for the SEPIC are shown in equations (1) through (4).

$$\frac{dI_{L_1}}{dt} = \frac{V_{C_{in}}}{L_1} + \frac{V_{C_s} + V_{C_{out}}}{L_1} \cdot (S_1 - 1) \quad (1)$$

$$\frac{dI_{L_2}}{dt} = \frac{V_{C_s}}{L_2} \cdot S_1 + \frac{V_{C_{out}}}{L_2} \cdot (S_1 - 1) \quad (2)$$

$$\frac{dV_{C_s}}{dt} = \frac{I_{L_1}}{C_s} \cdot (1 - S) - \frac{I_{L_2}}{C_s} \cdot S \quad (3)$$

$$\frac{dV_{C_{out}}}{dt} = \frac{I_{L_1} + I_{L_2}}{C_{out}} \cdot (1 - S) - \frac{V_{C_{out}}}{C_{out} \cdot R_{out}} \quad (4)$$

In these equations, S is the status of the switch (1 for ON, 0 for OFF), I_{L1} is the current through the inductor L_1, and I_{L2} is the current through the inductor L_2. V_{Cin} is the voltage across the capacitor C_{in}, V_{Cs} is the voltage across the capacitor C_s, and V_{Cout} is the voltage across the capacitor C_{out}. R_{out} represents the equivalent loads that can be connected at the output of the converter. The following design parameters are chosen for the SEPIC to operate as a SAR in the system. Inductive and capacitive elements are selected through SEPIC design equations [13] and empirical tuning within the simulation environment.

TABLE II:
SEPIC CONVERTER DESIGN PARAMETERS

Variable	*Description*	*Value*	*Unit*
V_{PV}	*Nominal PV Array Voltage*	180	*V*
V_{BUS}	*Nominal Bus Voltage*	120	*V*
I_{out}	*Maximum Output Current*	150	*A*
f_{sw}	*Nominal Switching Frequency*	100	*kHz*
C_{in}	*Input Capacitor*	470	*μF*
L_1, L_2	*Energy Storage Inductors*	100	*μH*
C_s	*Series Capacitor*	10	*μF*
C_{out}	*Output Capacitor*	100	*μF*

C. Battery Charge-Discharge Unit (BCDU)

The BCDU uses a bidirectional converter state-space model, realized as either a synchronous buck or boost converter, providing current flow and voltage conversion between the BESS and main bus during periods of charge and discharge. The bidirectional converters topology is composed of an inductor, a capacitor, and two switching transistors. Fig. 5 illustrates the buck-boost bidirectional converter circuit schematic.

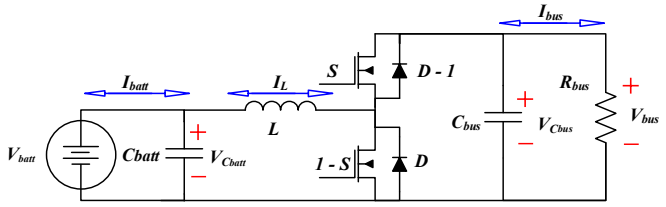

Fig. 5. The bidirectional converter circuit schematic. The converter allows charging and discharging the energy storage system.

Performing an analysis on the ON and OFF switching states of the buck-boost bidirectional converter, the dynamic equations can be obtained and are shown in equations (5) through (7).

$$\frac{dI_L}{dt} = \frac{V_{C_{batt}}}{L} - \frac{V_{C_{bus}}}{L} \cdot (1 - S) \tag{5}$$

$$\frac{dV_{C_{batt}}}{dt} = \frac{I_{batt}}{C_{batt}} - \frac{I_L}{C_{batt}} \tag{6}$$

$$\frac{dV_{C_{bus}}}{dt} = \frac{I_L}{C_{bus}}(1 - S) - \frac{V_{C_{bus}}}{C_{bus} \cdot R_{bus}} \tag{7}$$

In these equations, S is the status of the switch (1 for ON, 0 for OFF) and I_{L3} is the current through the inductor L_3. V_{Cbatt} is the voltage across the battery capacitor C_{batt} and V_{Cbus} is the voltage across the capacitor C_{bus}. V_{batt} is the battery voltage and I_{batt} is the battery current. R_{bus} represents the equivalent loads that can be connected at the bus-side of the converter. Table III summarizes the parameters chosen for the bidirectional converter to operate as a BCDU in the system. Inductive and capacitive elements are selected through design equations [14, 15] and empirical tuning within the simulation environment.

TABLE III:
BATTERY CHARGE-DISCHARGE UNIT DESIGN PARAMETERS

Variable	*Description*	*Value*	*Unit*
V_{batt}	*Nominal Battery Voltage*	145	*V*
V_{bus}	*Nominal Bus Voltage*	120	*V*
f_{sw}	*Nominal Switching Frequency*	100	*kHz*
C_{batt}	*Battery Capacitor*	100	*μF*
L	*Energy Storage Inductor*	10	*μH*
C_{bus}	*Bus Capacitor*	100	*μF*

To provide charge and discharge capability through the BCDU, a droop controller with a current-controlled output is implemented within the simulation environment. This control method consists of a PI-controller regulating the converter's duty cycle based on measured current feedback and output bus voltage values. As detailed later, the current set points for the controller are modified during run-time through the hierarchical control scheme to optimize battery State-of-Charge (SoC).

D. Battery Energy Storage System (BESS)

The BESS battery model is a standard offering from the *Simscape* Specialized Power Systems toolbox. A lithium-ion battery model with nominal electrical parameters is selected. The BESS voltage, capacity, and SoC parameters are chosen to provide adequate power delivery during absence of SA-generated power, while still being small enough to charge during typical lunar habitat load and irradiance conditions.

TABLE IV:
BATTERY ENERGY STORAGE SYSTEM PARAMETERS

Variable	*Description*	*Value*	*Unit*
V_{nom}	*Nominal Voltage*	145	*V*
RC	*Rated Capacity*	62.5	*Ah*
SoC	*Initial State-of-Charge*	50	*%*
V_{max}	*Fully charged Voltage*	157.1	*V*
V_{min}	*Cut-off Voltage*	101.2	*V*
R_{int}	*Internal Resistance*	0.02	*Ω*

E. DC-DC Converter Unit (DDCU)

The DDCU is modeled as a buck converter, capable of regulating the voltage output and providing unidirectional current flow from the main bus to the PDU loads. The model consists of the state-space equations for the buck converter and a PI controller to regulate the output voltage. The buck converter topology is composed of a capacitor, an inductor, a switching transistor, and a diode. Fig. 6 illustrates the buck converter circuit schematic.

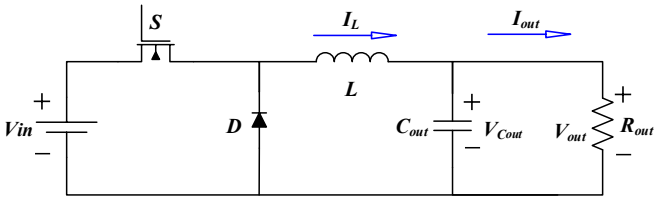

Fig. 6. The buck converter circuit schematic. The buck converter allows for lower voltage levels at its output.

To obtain the dynamic equations that model the buck converter's behavior, a simple analysis of the ON and OFF states is performed on the circuit. The dynamic equations of the converter are shown in equations (8) and (9).

$$\frac{dI_L}{dt} = \frac{V_{C_{in}}}{L} \cdot S - \frac{V_{C_{out}}}{L} \tag{8}$$

$$\frac{dV_{C_{out}}}{dt} = \frac{I_L}{C_{out}} - \frac{V_{C_{out}}}{C_{out} \cdot R_{out}} \tag{9}$$

In these equations, S is the status of the switch (1 for ON, 0 for OFF), I_L is the current through the inductor L, while V_{Cout} is the voltage across the capacitor C_{out}. R_{out} represents the equivalent loads that can be connected at the output of the converter. The following parameters are chosen for the buck converter to operate as a DDCU in the system. Inductive and capacitive elements are selected through the buck converter's design equations [15] and empirical tuning within the simulation environment.

TABLE V:
DDCU DESIGN PARAMETERS

Variable	*Description*	*Value*	*Unit*
V_{in}	*Nominal Input Voltage*	≥120	*V*
V_{out}	*Nominal Output Voltage*	120	*V*
I_{out}	*Nominal Output Current*	25	*A*
f_{sw}	*Nominal Switching Frequency*	100	*kHz*
L	*Energy Storage Inductor*	25	*μH*
C_{out}	*Output Capacitor*	10	*μF*

Each DDCU supplies power to the PDU and power and propulsion element (PPE) loads. There are six loads, each consuming 3 kW with an additional load step of 200 W at a constant 10 Hz rate. The load stepping is intended to test the transient power handling alongside the constant 3 kW power draw. For this simulation, main bus switching units (MBSU) and secondary bus switching units (SBSU) are held in static 'ON' states to provide maximum power to the loads without disruption.

IV. Proposed Hierarchical Control

Hierarchical control schemes for the BESS can be employed to achieve a more resilient power architecture than localized control alone. *Level 1* (primary) is a local droop controller that regulates power and voltage to the system, while *Level 2* and *Level 3* (secondary and tertiary) use battery SoC and power flow data to provide control setpoints for each distributed BESS [1]. This research offers many practical considerations for how high-level control over BESSs will allow for longevity and resiliency within lunar power systems.

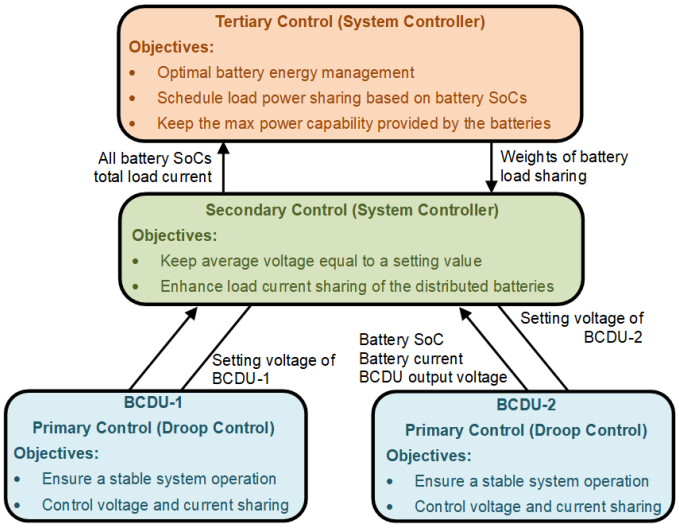

Fig. 7. Block Diagram of the Hierarchical Control Scheme.

The implementation of hierarchical control for this research relies on the battery SoC to determine the amount of current that can be charged or discharged from the battery at a given time. To preserve battery capacity, the BCDU's current controller adopts new maximum setpoints deployed from the system controller. The hierarchy to our simulation and hardware model control is as follows (highest to lowest level of control):

- **Tertiary Control:** Battery SoC is passed into system controller to determine BCDU control set points.
- **Secondary Control:** Droop controller's current set point determines average duty cycle value of the converter.
- **Primary Control:** Average duty cycle value sets PWM waveform to converter for power transfer.

Setpoints for the BCDU are defined as such for the hardware converter model to be tested. By varying the charge rate based on SoC, the hierarchical control is capable of further protection the battery and controlling overall power flow within the system.

TABLE VI:
HIERARCHICAL CONTROL BCDU SETPOINTS

SoC (%)	$I_{charge,max}$ *(A)*	$I_{discharge,max}$ *(A)*
>90	5.21	41.67
70 - 90	10.42	41.67
50 - 70	20.84	41.67
30 - 50	41.67	20.84
10 - 30	41.67	10.42
< 10	41.67	5.21

V. Simulation Results

Developing the entire lunar habitat model in simulation provides a comprehensive platform for which the BCDU control can be tested in the PHIL environment. Fig. 8 shows the simulated power flow of the BESS units in the lunar habitat without the use of a hierarchical control for the BCDUs. The SoC and power flow from identical BESSs are disproportionate in the system during both the charge and discharge states. (an eclipse event is demonstrated at 30 sec). It is desired that battery units either have equivalent power flow or uniform SoC during their operation. This can be achieved through more advanced control methods proposed.

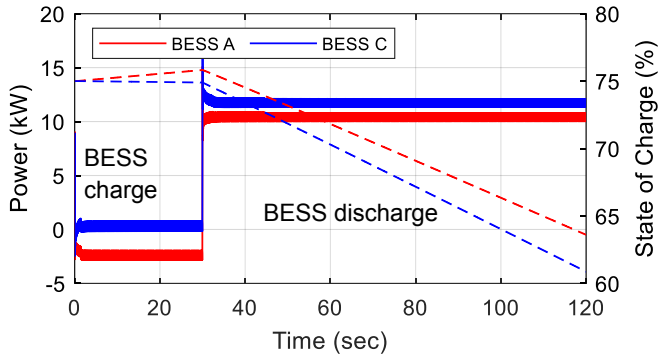

Fig. 8. BESS Power Flow and SoC Without Hierarchical Control.

By implementing new droop controller setpoints periodically during simulation runtime shows that there exists a benefit to ensuring SoC uniformity between multiple BESS systems. The hierarchical control scheme observes power flow and SoC metrics, adjusting the BCDU droop controller over time. Fig. 9 captures this behavior with a setpoint adjustment to BESS C at 60 sec. The droop controller setpoints adjustments allow variation in battery output power and guarantees uniform SoC over time.

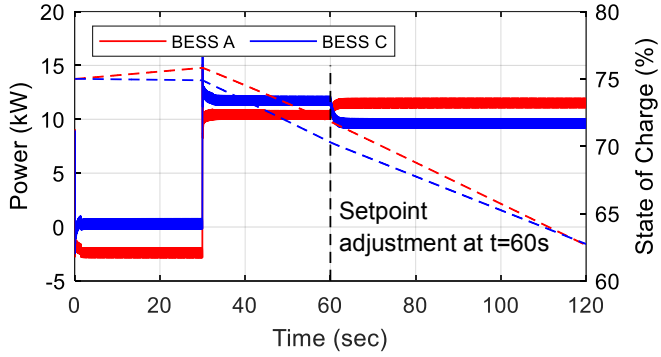

Fig. 9. BESS Power Flow and SoC with Hierarchical Control.

This control method provides a novel approach to ensuring reliable BESS power conversion within the DC microgrid (via localized droop controllers) as well as uniformity in battery power flow and discharge (via hierarchical control). The next steps towards experimental results will is to incorporate the hierarchical BCDU control model into the real-time simulation environment using the Opal-RT PHIL platform and a replacing the simulated bidirectional converter with a physical bidirectional DC/DC converter.

VI. Real-Time Simulation and Hardware Results

The experimental test setup, shown in Fig. 10, is prepared for the simulation and BCDU converter using a PHIL platform. To test both charge and discharge capabilities, as well as transient response of the physical BDCU converter, during source disruptions, an eclipse event is introduced halfway through the simulation time. The eclipse event causes an instantaneous loss of power from the SA to the lunar habitats main bus. This not only tests the BESS capability to provide power to the load, but also captures the ability for the BCDU controller to switch from charge to discharge modes.

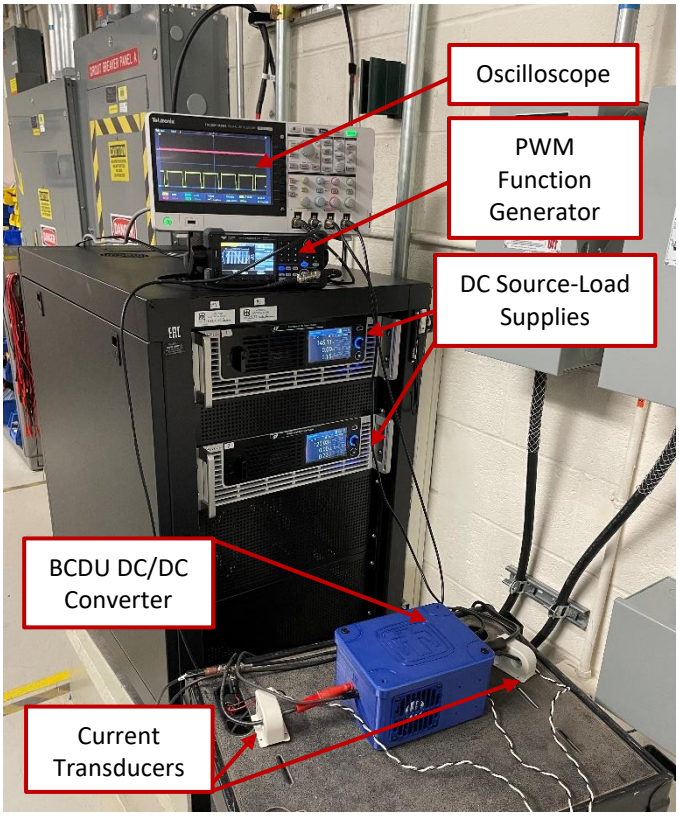

Fig. 10. Power Hardware-in-the-Loop Experimental Setup for testing the BCDU Converter. In this test setup, the lunar habitat is simulated in the Opal-RT real-time simulator to test BCDU performance.

The current set points of the hardware BCDU controller are modified by the system controller to preserve battery SoC. The primary control adjusts to implement the newly dispatched current set points throughout the simulation. These control changes are detailed as phases in the simulation (1-4) based on the power provided from the SA and system controller updates to the hardware BCDU interfacing with BESS B. Fig. 11 illustrates the power flow and SoC of the hardware-based BESS alongside the simulation models. For this test, the system controller only provides updates to the BCDU B. Omitting the hierarchical control from all other BCDUs allows for a more controlled test environment for the hardware converter. Table VII details the average power values for each power source/load during each test phase.

TABLE VII:
AVERAGE POWER CONTRIBUTIONS DURING RUN-TIME

	Full Irradiance / BESS Charge (W)		***Eclipse / BESS Discharge (W)***	
Power Source/Load	***Phase 1 0-120s***	***Phase 2 120-240s***	***Phase 3 240-360s***	***Phase 4 360-480s***
SA	37278	37296	0	0
BESS A	-6149	-6157	4175	4757
BESS B (PHIL)	-6141	-3052	4168	3005
BESS C	-1894	-3456	5184	5472
BESS D	-1894	-3456	5184	5472
Load	18686	18686	18533	18522

Under full irradiance conditions, BESS B matches BESS A output power until the SoC reaches 50%. At this point, the system controller dispatches a new current set point to the BCDU B controller. The charge current for the BESS reduces by half and causes other BESS units to charge at a higher rate. BESS A and B are shown to charge at a higher rate due to their proximity in the SAF (as compared to BESS C and D located across the SAF-habitat interconnect). During eclipse events, the BESS units switch to discharge to support the lunar habitat load. Phase 3 matches output power between BESS A and B and BESS C and D. BESS C and D provide additional power due to their proximity to the lunar habitat loads (shown overlapping in Fig. 11). In Phase 4, BESS B's discharge rate reduces due to the SoC of the battery dropping below 50%. The BCDU current setpoints lower to preserve the battery's capacity under the current load conditions. Phase 4 shows all other BESS units increasing their output power to support the lunar habitat load.

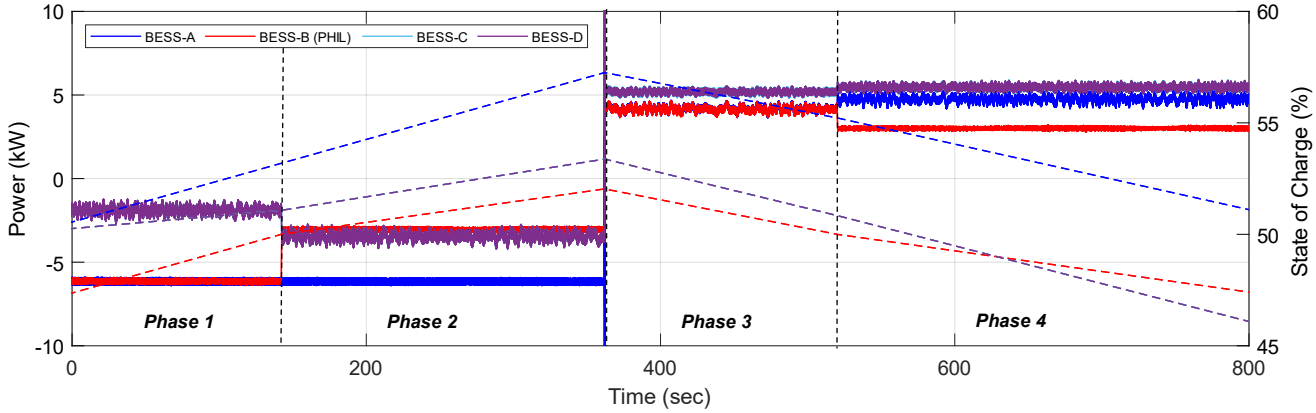

Fig 11. Results for Power Flow and State-of-Charge of BESS Units During Real-Time Simulation.

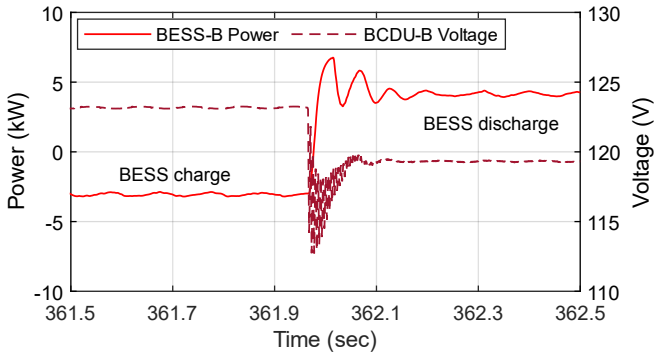

Fig. 12. Results of BESS B Transient Response During Eclipse Event.

The transient performance of the simulation shows stability throughout, though the eclipse condition is further examined. Fig. 12 shows the power and voltage performance of the BESS B unit as the BCDU controller shifts from charge to discharge modes. Some ringing is present in this transition, however the BCDU does reach a steady state within 500 msec. With further tuning of the BCDU droop controller, better transient performance could be obtained.

VII. Conclusion

A hierarchical control scheme for a lunar habitat's DC microgrid is proposed and implemented through a real-time simulation and PHIL environment. State-space average models are developed in *MATLAB/Simulink* that represent the lunar habitat microgrid's power converters. Environmental conditions, such as eclipses and power line impedances, are examined in simulation and through experimental testing. Developing a PHIL platform for DC hardware devices provides the ability for more critical testing. By integrating DC source-load power supplies and current transducers into the Opal-RT's real-time simulation environment, power hardware devices are tested as part of the lunar habitat with scenarios previously only tested in simulation. Furthermore, the real-time simulation introduces both primary and hierarchical control of the BCDU and tests its power sharing capability alongside all other lunar habitat models. Next steps for this work can involve more comprehensive hierarchical control methods that consider SoC control of both hardware and software BCDU models. Additionally, the DC-PHIL platform can be further expanded to include testing of more realistic power hardware devices intended for lunar and aerospace applications.

Acknowledgement

Sandia National Laboratories is a multi-mission laboratory managed and operated by National Technology and Engineering Solutions of Sandia, LLC., a wholly owned subsidiary of Honeywell International, Inc., for the U.S. Department of Energy's National Nuclear Security Administration under contract DE-NA-0003525.

The NASA Glenn Research Center, and NTESS of Sandia, LLC collaborate in accordance with the National Aeronautics and Space Act (51 U.S.C. § 20113(e)) under contract SAA3-1690.

References

[1] J. Zhang, J. T. Csank and J. F. Soeder, "Hierarchical Control of Distributed Battery Energy Storage System in a DC Microgrid," *2021 IEEE Fourth International Conference on DC Microgrids (ICDCM)*, 2021, pp. 1-8.

[2] L. Bowling, B. Horvath and C. Wohl, "Integration of Advanced Structures and Materials Technologies for a Robust Lunar Habitat," *2021 IEEE Aerospace Conference*, 2021, pp. 1-13.

[3] G. Flores, D. Harris, R. McCauley, S. Canerday, L. Ingram and N. Herrmann, "Deep Space Habitation: Establishing a Sustainable Human Presence on the Moon and Beyond," *2021 IEEE Aerospace Conference (50100)*, 2021, pp. 1-7.

[4] A. D. Bintoudi, C. Timplalexis, G. Mendes, J. M. Guerrero and C. Demoulias, "Design of Space Microgrid for Manned Lunar Base: Spinning-in Terrestrial Technologies," *2019 European Space Power Conference (ESPC)*, 2019, pp. 1-8

[5] L. Wang, D. Zhang, J. Duan and J. Li, "Design and Research of High Voltage Power Conversion System for Space Solar Power Station," *2018 IEEE International Power Electronics and Application Conference and Exposition (PEAC)*, 2018, pp. 1-5.

[6] M. D'Antonio, C. Shi, B. Wu and A. Khaligh, "Design and Optimization of a Solar Power Conversion System for Space Applications," in *IEEE Transactions on Industry Applications*, vol. 55, no. 3, pp. 2310-2319, May-June 2019.

[7] K. G. Boggs, K. Goodliff and D. Elburn, "Capabilities Development: From International Space Station and the Moon to Mars," *2020 IEEE Aerospace Conference*, 2020, pp. 1-10.

[8] K. G. Boggs and K. D. Foley, "International space station testbed for exploration," *IEEE Aerospace Conference*, 2018, pp. 1-6.

[9] R. Darbali-Zamora and E. I. Ortiz-Rivera, "A State Space Average Model for Dynamic Microgrid Based Space Station Simulations," *2017 IEEE 44th Photovoltaic Specialist Conference (PVSC)*, 2017, pp. 2957-2962.

[10] M. Kaczmarzyk and M. Musiał, "Parametric Study of a Lunar Base Power Systems," *Energies*, vol. 14, no. 4, p. 1141, Feb. 2021

[11] G. V. Somanath Reddy, V. P. Mini, N. Mayadevi and R. Hari Kumar, "Optimal Energy Sharing in Smart DC Microgrid Cluster," *2020 IEEE International Conference on Power Electronics, Smart Grid and Renewable Energy (PESGRE)*, 2020, pp. 1-6,

[12] Yu, S.-Y.; Kim, H.-J.; Kim, J.-H.; Han, B.-M. SoC-Based Output Voltage Control for BESS with a Lithium-Ion Battery in a Stand-Alone DC Microgrid. *Energies* 2016, 9, 924.

[13] D. Zhang, "AN-1484 Designing A SEPIC Converter", *Texas Instruments*, Apr. 2013. [Online]. Available: https://www.ti.com/lit/an/snva168e/snva168e.pdf [Accessed: October 2021]

[14] B. Hauke, "Basic Calculation of a Boost Converter's Power Stage", *Texas Instruments*, Jan. 2014. [Online]. Available: https://www.ti.com/lit/an/slva372c/slva372c.pdf [Accessed: October 2021]

[15] B. Hauke, "Basic Calculation of a Buck Converter's Power Stage", *Texas Instruments*, Aug. 2015. [Online]. Available: https://www.ti.com/lit/an/slva477b/slva477b.pdf [Accessed: October 2021]

[16] R. Darbali-Zamora and E. I. Ortiz-Rivera, "Optimal duty ratio maximum power point tracking technique using the SEPIC topology for photovoltaic systems applications," 2016 IEEE ANDESCON, 2016, pp. 1-4, doi: 10.1109/ANDESCON.2016.7836257.

[17] "Using the LMG3410-HB-EVM Half-Bridge and LMG34XX-BB-EVM Breakout Board EVM", *Texas Instruments*, May 2017. [Online]. Available: https://www.ti.com/lit/ug/snou140a/snou140a.pdf [Accessed: May 2022]

[18] R. Darbali-Zamora, N. Cobo-Yepes, J. E. Salazar-Duque, E. I. Ortiz-Rivera and A. A. Rincon-Charris, "Buck Converter and SEPIC Based Electronic Power Supply Design with MPPT and Voltage Regulation for Small Satellite Applications," 2017 IEEE 44th Photovoltaic Specialist Conference (PVSC), 2017, pp. 2963-2968.